A comprehensive survey of alkaline electrolyzer modeling: electrical domain and specific electrolyte conductivity

Frank Gambou, Damien Guilbert, Michel Zasadzinski, Hugues Rafaralahy

energies

MDPI

Review

A comprehensive survey of alkaline electrolyzer modeling: electrical domain and specific electrolyte conductivity

Frank Gambou [1], Damien Guilbert [1,*], Michel Zasadzinski [2] and Hugues Rafaralahy [2]

1 Group of Research in Electrical Engineering of Nancy (GREEN), University of Lorraine, F-54000 Nancy, France, frank.gambou@univ-lorraine.fr (F.G.), damien.guilbert@univ-lorraine.fr (D.G.);
2 Research Center for Automatic Control of Nancy (CRAN), (UMR CNRS 7039), University of Lorraine, F-54000 Nancy, France, michel.zasadzinski@univ-lorraine.fr, hugues.rafaralahy@univ-lorraine.fr (H.R.);
* Correspondence: damien.guilbert@univ-lorraine.fr, Tel.: +33-372-749-984

Abstract: Alkaline electrolyzers are the most widespread technology due to their maturity, low cost, and large capacity in generating hydrogen. However, compared to proton exchange membrane (PEM) electrolyzers, they request the use of potassium hydroxide (KOH) or sodium hydroxide (NaOH) since the electrolyte relies on a liquid solution. For this reason, the performances of alkaline electrolyzers are governed by the electrolyte concentration and operating temperature. Due to the growing development of the water electrolysis process based on alkaline electrolyzers to generate green hydrogen from renewable energy sources, the main purpose of this paper is to carry out a comprehensive survey on alkaline electrolyzers, and more specifically about their electrical domain and specific electrolytic conductivity. Besides, this survey will allow emphasizing the remaining key issues from the modeling point of view.

Keywords: Alkaline electrolyzer; hydrogen generation; modeling; dynamic operation; electrolyte conductivity

1. Introduction

Fossil-based energy sources such as coal, oil, and natural gas have been used for several centuries as primary energy sources. However, their consumption are releasing millions of tonnes of CO_2 every year, resulting in air pollution and a greenhouse gas phenomenon [1]. In addition, their future depletion leads to imagining their replacement by renewable energy sources (RES) to protect the environment from climate change. For this purpose, hydrogen seems to be the best and most suitable alternative for fossil-based energy sources since its consumption does not emit CO_2 but produces only water [2,3]. This makes hydrogen one of the cleanest fuels in the world and essential for achieving a pollution-free by 2050 according to the European Union's (EU) commitment. Unfortunately, its production is still largely dominated using fossil fuels (specifically natural gas) [4–7]. Only a small amount is produced through the water electrolysis process which uses electricity to split water into hydrogen and oxygen. To contribute to climate neutrality, hydrogen production must require electricity coming from RES such as wind, solar, geothermal, biomass, or nuclear [1]. As hydrogen is applied in various energy-intensive sectors such as transport, industry, electricity, and construction, it offers enormous solutions in the reduction of greenhouse gas emissions [6,8]. For this reason, the hydrogen strategy set by the EU is to install in Europe at least 6 GW of renewable hydrogen electrolyzers by 2024, and 40 GW by 2030 [7]. Hence, the goal is to decrease greenhouse gas emissions by at least 55% by 2030.

Electrolyzers are electrochemical devices used to produce hydrogen through water electrolysis. At the present moment, there are four electrolyzers technologies: alkaline

Citation: Gambou, F.; Guilbert, D.; Zasadzinski, M; Rafaralahy, H. A comprehensive survey of alkaline electrolyzer modeling: electrical domain and specific electrolyte conductivity. *Energies* **2022**, *15*, x. https://doi.org/10.3390/xxxxx

Academic Editor: Firstname Lastname

Received: date
Accepted: date
Published: date

electrolyzer, proton exchange membrane (PEM) electrolyzer, solid oxide (SO) electrolyzer, and anion exchange membrane (AEM) electrolyzer recently introduced in the literature to eliminate the weaknesses of alkaline and PEM electrolyzers [1,9,10]. Only the two first technologies are commercially available in the market and widely used; while the two remaining are still under investigation since they are not enough mature to be accepted and employed in research projects [10].

The alkaline electrolyzer technology has been used for over a century. Its principle is based on the use of two electrodes immersed in an electrolyte solution of potassium hydroxide (KOH) or sodium hydroxide (NaOH). A membrane called the diaphragm separates the two electrodes and allows the hydroxide ions (OH^-) to move from the cathode to the anode [11,12]. The advantage of this technology is that the electrodes are made of cheaper catalysts such as cobalt, nickel, or iron. Also, it has high durability and gas purity [9]. Unfortunately, it operates at a low current density lying between 0.2 and 0.7 A.cm^2, making it less compact than PEM electrolyzers. Furthermore, the production capacity dynamic range is set between 15 and 100% which prevents alkaline electrolyzers to be fully exploited in RES operations. Finally, the aqueous solution of the electrolyte (KOH or NaOH) leads up to regular checks and maintenance to guarantee safe operations and the performance of the system [9].

The PEM electrolyzers were first developed in the 1960s to overcome some of the disadvantages of the alkaline electrolyzer. They are composed of a solid polymer electrolyte (SPE) separating the anode from the cathode and allowing protons (H^+) to be diffused from the anode to the cathode. The catalyst material on the anode and the cathode side are respectively iridium and platinum, which are noble and expensive materials [3]. On one hand, the main advantages of this technology over alkaline technology are high current densities, low maintenance, and large production capacity dynamic range (0-100 %) [13]. On the other hand, the output hydrogen pressure is quite limited (around 30 bars); whereas for alkaline electrolyzers, the pressure can go up to 200 bars at the same rated power. Given that this technology has not yet reached a certain level of maturity, its performances (e.g., specific energy consumption, hydrogen production rate, lifespan) are below those met by alkaline electrolyzers. For this reason, this technology is currently being investigated by researchers to compete from the performance point of view with alkaline electrolyzers [14].

Recently, several review works have been reported for PEM electrolyzers. These reviews deal with modeling aspects, novel components, cell failure mechanisms, and technology [2,3,15–17]. On the other side, a few reviews can be found for alkaline electrolyzers. In [9], the authors have focused their investigation on the technology while providing research perspectives to enhance its performance and dissemination. In comparison, in [18], the authors have reviewed and analyzed the coupling between alkaline electrolyzers and RES (wind, solar). Relying on the current literature, the main goal of this paper is to review alkaline electrolyzer modeling from the electrical domain point of view. Besides, given that the alkaline electrolyzer performances are strongly linked with the specific electrolyte conductivity of the aqueous solution, their modeling according to the temperature and mass fraction of KOH or NaOH is considered in this review work. Hence, it allows bringing out the remaining key issues from the modeling point of view.

The paper is divided into four sections. After reviewing alkaline and PEM technologies while highlighting the reported review works on both technologies, section 2 summarizes the principle of operation, features, static and dynamic operations of alkaline electrolyzers. Then, in the third section, a detailed synthesis of alkaline electrolyzer modeling including electrical domain and specific electrolyte conductivity is provided. Finally, in section 4, a conclusion is provided enabling giving the remaining key issues for alkaline electrolyzer modeling.

2. Alkaline Electrolyser Technology

2.1. Operation and characteristics

As pointed out in the introduction, among the four existing water technologies, only two are available in the market such as alkaline, PEM; whereas SO and AEM are still being investigated before widespread acceptance and dissemination [19,20]. In this review work, alkaline water electrolysis technology is considered since it is currently being employed in many research projects such as the development of carbon-free hydrogen production facilities supplied by renewable sources [21,22]. Similar to fuel cells, electrolyzers performing the water electrolysis process are composed of an anode and a cathode separated by an electrolyte. In the case of the alkaline electrolyzer, the electrolyte is based on a liquid solution that may be potassium hydroxide (KOH) or sodium hydroxide (NaOH) [9]. Generally, alkaline electrolyzer manufacturers prefer to use KOH instead of NaOH since an aqueous solution with 25-30 wt. % KOH features a higher specific electrolyte conductivity at a standard temperature range from 50 to 80°C [18]. The principle of operation of the alkaline water electrolysis is provided in Figure 1; while the equations of the chemical reactions are given in Equations (1)-(3) below:

$$\text{Anode:} \quad 2OH^- \rightarrow \tfrac{1}{2}O_2 + H_2O + 2e^- \tag{1}$$

$$\text{Cathode:} \quad 2H_2O + 2e^- \rightarrow H_2 + 2OH^- \tag{2}$$

$$\text{Global:} \quad 2H_2O \rightarrow 2H_2 + 2O_2 \tag{3}$$

Based on Figure 1 and the chemical reactions, pure water mixed with KOH is supplied at the cathode side. The water reacts with electrons generating hydroxide ions (OH^-) and hydrogen (H_2) at the cathode side. Then, hydroxide ions are transported to the anode side through the liquid electrolyte, whereas electrons migrate to the anode side via the gas diffusion layer (GDL). On the anode side, oxygen is produced.

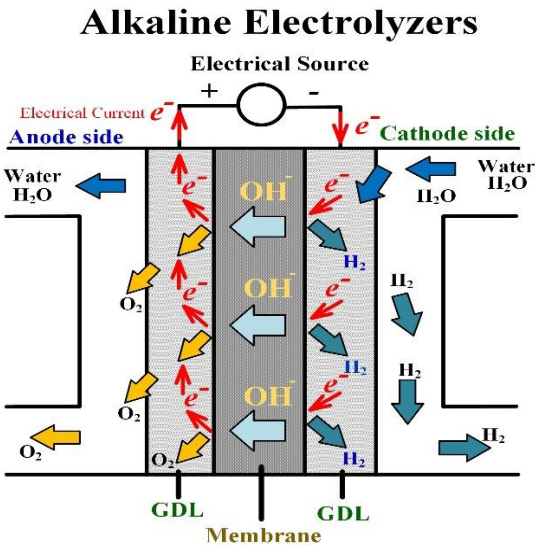

Figure 1. Principle of operation of alkaline electrolyzers.

To highlight the strengths, weaknesses, opportunities, and threats of alkaline technology, a SWOT analysis has been carried out and reported in Table 1. Despite alkaline technology features several advantages, it presents several weaknesses such as limited current density, frequent maintenance (liquid electrolyte), and limited production capaci-

ty dynamic range [6]. However, some opportunities might enhance the performance and hydrogen production of the technology by using new materials and designing stacks differently [23,24]. Moreover, the growing interest from industry and researchers in PEM electrolyzers might threaten the widespread dissemination of alkaline electrolyzers. Indeed, PEM electrolyzers have been introduced in the 1960s to compete with alkaline electrolyzers to eliminate some of their disadvantages cited above. They present several benefits over alkaline electrolyzers from the current density, maintenance, and production capacity dynamic range point of view [3].

Table 1. SWOT analysis with strengths, weaknesses, opportunities, and threats of alkaline water electrolysis technology.

STRENGTHS	**WEAKNESSES**
✓ Low cost (due to cheaper catalyst materials such as Nickel (Ni)) ✓ High lifetime and gas purity ✓ High hydrogen production capacity (up to 3880 $Nm^3.h^{-1}$) ✓ Low specific energy consumption (around 3.8 $kWh.Nm^{-3}$)	✓ Limited current density (0.2-0.7 $A.cm^{-2}$) ✓ Frequent maintenance requested (due to the use of a liquid electrolyte solution) ✓ Limited production capacity dynamic range (15-100 %)
OPPORTUNITIES	**THREATS**
✓ Increase in the use of non-precious metals (Co, Fe, Mn, Cr, Cu, and Zn) combined with Ni to enhance the performance ✓ Design in spacing electrodes to optimize hydrogen production ✓ Dissemination of low carbon footprint hydrogen production plants supplied by renewable and nuclear resources	✓ Growing development of PEM water electrolysis technology due to its benefits (high current density and efficiency, large production capacity dynamic range, low maintenance) ✓ Lack of hydrogen refueling stations close to the hydrogen production units

Finally, relying on the current state-of-the-art (research papers, alkaline electrolyzer manufacturers) [8,18] Table 2 summarizes the main features of alkaline technology. From Table 2, it can be noted that alkaline electrolyzers can generate hydrogen at very high pressure (up to 200 bar against 30 bar for PEM electrolyzers at the same rated power of 2 MW from NEL company). High-pressure hydrogen production is an important issue since hydrogen is stored under gaseous form at 700 bar in storage tanks embedded in commercial fuel cell electric vehicles (FCEVs) [25]. In any case, compressors are requested to meet the high-pressure requirements of FCEVs. Furthermore, since the technology is mature over PEM electrolyzers, the best performance can be obtained such as low specific energy consumption, high hydrogen volume rate, and lifetime. The main drawbacks reported concern the low current density (up to 0.7 $A.cm^{-2}$ making the electrolyzer bulky) and set production capacity dynamic range (limiting operating conditions to generate hydrogen). The system efficiency is assessed by considering the stack efficiency range and the losses from power electronics (around 5%) with the use of AC-DC converters such as thyristors or transistors-based rectifiers [26,27].

Table 2. Summary of features for alkaline water electrolysis technology.

Specification	Alkaline Electrolyzer
Electrolyte	25-30 % KOH aqueous solution
Cell temperature	60–80 °C
Gas purity	99.999 %
Pressure	1–200 bar
Current density	0.2–0.7 $A.cm^{-2}$
Cell voltage	1.6–2.6 V
Cell voltage efficiency (LHV[1])	58–77 %
Stack voltage	18–522 V
Stack Current	60–5250 A
System efficiency	55-73%
Specific energy consumption at stack	3.8–4.4 $kWh.Nm^{-3}$
Production capacity dynamic range	15–100%
Cell area	≤ 770 m^2
Hydrogen production rate	1.5–3880 $Nm^3.h^{-1}$
Hydrogen volume rate	Up to 8374 kg/24h
Lifetime stack	< 90,000 h (more than 10 years)
Lifetime system incl. maintenance	20 + years

[1]: Lower heating value (around 120 $MJ.kg^{-1}$).

2.2. Static and dynamic operation

Before reviewing the electrical domain modeling of alkaline electrolyzers in the next section, it is crucial to show their static and dynamic characterization. Hence, an experimental test bench has been realized at the GREEN laboratory, IUT de Longwy (France), to perform static and dynamic tests on a single cell alkaline electrolyzer as shown in Figure 2. The technical specifications of the electrolyzer are summarized in Table 3.

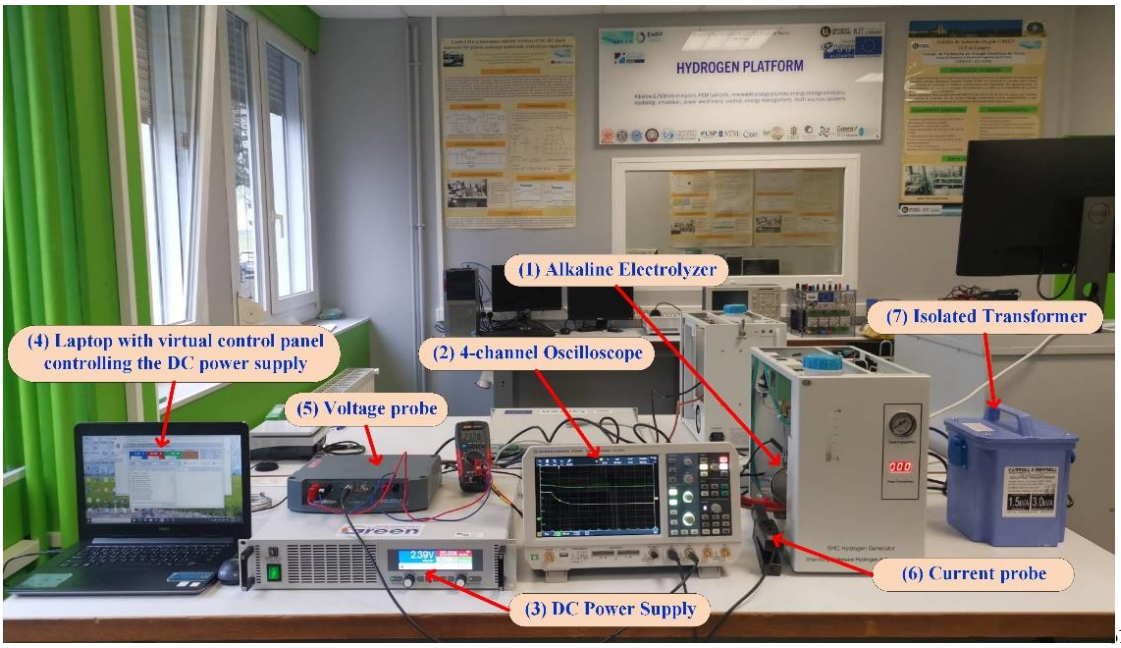

Figure 2. Experimental test bench for static and dynamic tests.

Table 3. Technical specification of the studied alkaline electrolyzer.

Parameters	Value	Unit
Rated electrical power	150	W
Operating voltage range	1.6-2.6	V
Current range	0-45	A
Delivery output hydrogen pressure	0.1-10.5	bar
Hydrogen purity	99.999	%
Cells number	1	-
Hydrogen volume range	0-310	$ml.min^{-1}$
Electrolyte	32 % weight KOH	-

The realized experimental test bench includes the following devices: (1) a single-cell alkaline electrolyzer, (2) a 4-channel oscilloscope, (3) a DC power supply, (4) a laptop enabling controlling the DC power supply for static and dynamic tests purposes, (5) a voltage probe to acquire the cell voltage of the electrolyzer, (6) a current probe to measure the cell current of the electrolyzer, and (7) an isolated transformer to eliminate the interference and noise from the power grid. To enable the good operation of the single-cell alkaline electrolyzer, 1000 ml of distilled water has been mixed with 32 % weight KOH as requested by the electrolyzer manufacturer. When the lye liquid has been fully melted, it has been put in a tank to supply the alkaline electrolyzer. Besides, the KOH purity is 85 %. Once the hydrogen is generated, it is stored in metal hydride storage tanks (not shown in Figure 2), enabling meeting safety recommendations for hydrogen storage.

First of all, the static characterization of the single-cell alkaline electrolyzer is depicted in Figure 3. This characterization allows emphasizing the two main overvoltage regions, the first from 0 to 2 A (activation region), and the second from 2 to 45 A (ohmic region). The reversible voltage at zero-current is roughly equal to 1.6 V. The ohmic overvoltage is influenced by different parameters such as the electrical conductivity of both electrodes (i.e., anode and cathode), the specific electrolyte conductivity, distances between the electrodes, and hydrogen and oxygen bubbles that cover some parts of the surface of the electrodes.

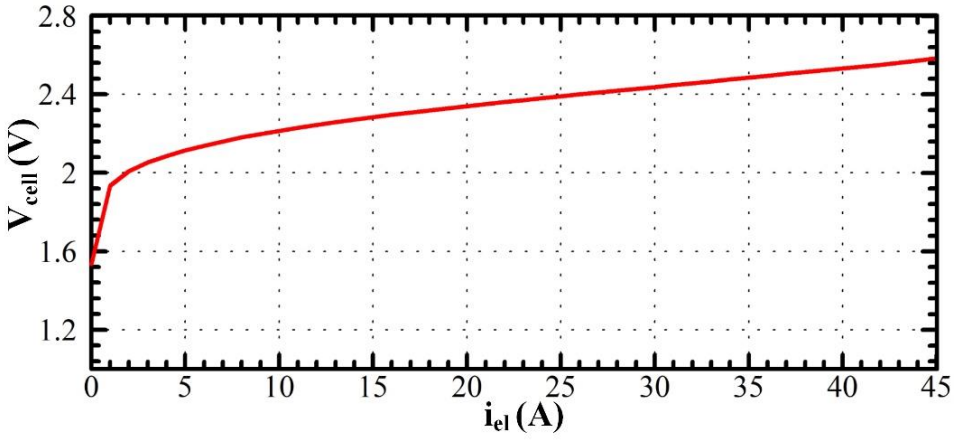

Figure 3. Static characterization of the studied alkaline electrolyzer.

After performing a static characterization of the alkaline electrolyzer, dynamic tests have been carried out. Rise and falling current steps (from 20 to 40 A, and inversely) have been applied to the single-cell alkaline electrolyzer. The results are shown respectively in Figure 4 and Figure 5. It can be noted that the single-cell alkaline electrolyzer responds quickly when changing operating conditions. Indeed, in both cases, the steady-state cell voltage operation is reached in 0.24 ms. Both tests demonstrate that the specific electro-

lyte conductivity is suitable to meet dynamic performance, as required when connecting alkaline electrolyzers to intermittent green energy sources such as RES [28].

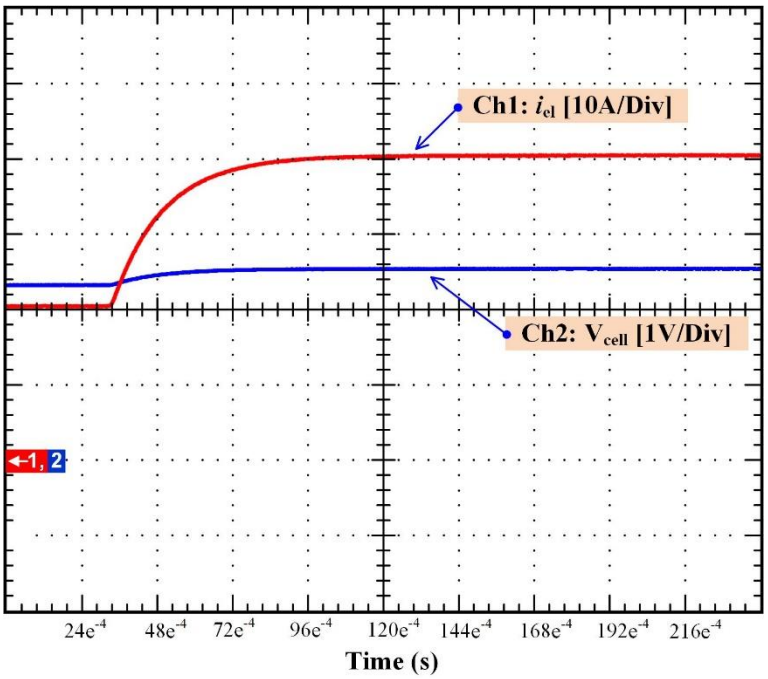

Figure 4. Dynamic test with a rise current step from 20 to 40 A.

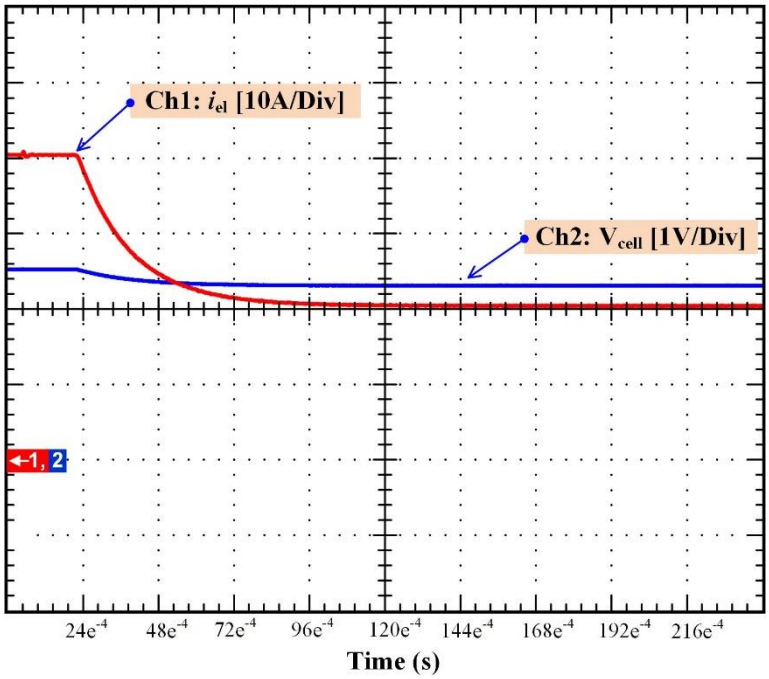

Figure 5. Dynamic test with a falling current step from 40 to 20 A.

Finally, a test with dynamic solicitations has been performed to highlight the performance of the studied alkaline electrolyzer. This test includes a rise current step (from 20 to 45 A) at 9 s, then a falling current step (from 45 to 10 A) at 32 s, and finally a rise current step (from 10 to 30 A) at 70 s as illustrated in Figure 6. In conclusion, dynamic performances are met when the alkaline electrolyzer is solicited by sudden operating conditions change.

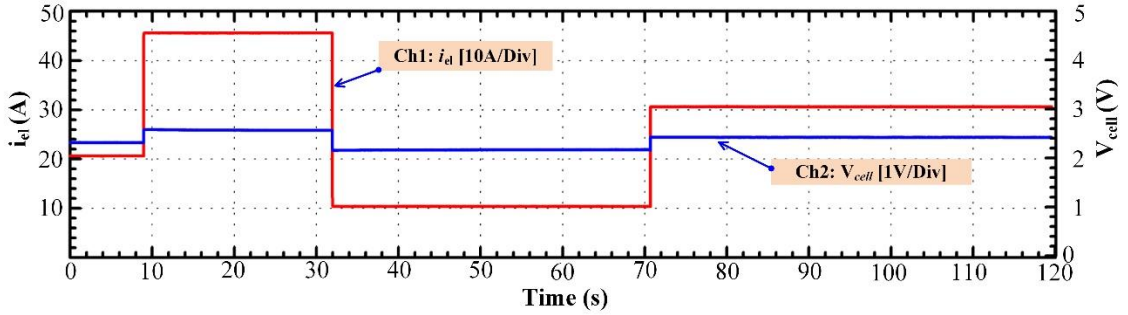

Figure 6. Tests with dynamic solicitations.

3. Electrical domain modeling

Over the last decades, the modeling of alkaline electrolyzers has attracted a lot of investigation from researchers to develop the use of this technology at a large scale powered by RES. However, as mentioned in the introduction, alkaline electrolyzers have received less modeling investigation than PEM electrolyzers. This difference may be explained by the benefits of using PEM electrolyzers over alkaline electrolyzers from the high current density, low maintenance, and large partial load range point of view. Besides, compared to PEM electrolyzers, no review works have been reported in the literature regarding alka-line electrolyzers modeling. Only two reviews can be found, dealing with the technology and its coupling with RES. Given that this review work is focused on electrical domain modeling, this section has been split into three main parts: semi-empirical, empirical, and dynamic modeling. This section aims at providing valuable information and guidelines to industrials, researchers, and students to model alkaline electrolyzers from the electrical domain point of view.

3.1. Static modeling

3.1.1. Introduction

First of all, the performance of the alkaline electrolyzer is linked to its polarization curve as shown in Figure 3. From Figure 3, the higher the current, the higher the cell voltage due to the overvoltages. At zero-current, the cell voltage is equal to the reversible voltage V_{rev}. At very low currents (up to 2 A), the activation overvoltages (anode and cathode) are preponderant, while from 2 A and above, the ohmic region is predominant. The reversible voltage, the activation, and the ohmic overvoltages depend strongly on the temperature, gas pressures, and the electrical conductivity of both electrodes (i.e., anode and cathode), the specific electrolyte conductivity, distances between the electrodes, and hydrogen and oxygen bubbles that envelops some areas of the surface of the electrodes. Hence, the cell voltage V_{cell} of the alkaline electrolyzer can be expressed by the general expression in Equation (4) below:

$$V_{cell} = V_{rev} + \eta_{ohm} + \eta_{act,a} + \eta_{act,c} \quad (4)$$

where V_{rev} (V) is the reversible voltage, η_{ohm} (V) is the ohmic overvoltage, $\eta_{act,a}$ (V) and $\eta_{act,c}$ (V) are respectively the activation overvoltage at the anode and the cathode.

In the next subsections, the semi-empirical, empirical, and dynamic modeling are detailed and analyzed.

3.1.2. Semi-empirical modeling

Several semi-empirical equations for alkaline electrolyzers have been used to model the current-voltage curve. One of the most used semi-empirical models was first described by Ulleberg [29]. The model combines thermodynamics, kinetics, and resistive ef-

fects of the electrolyzer. The basic form of the current-voltage curve is given in Equation (5) [18,29]:

$$V_{cell} = V_{rev} + r \cdot \left(\frac{i_{el}}{A_{elec}} \right) + s \cdot \log\left[t \cdot \left(\frac{i_{el}}{A_{elec}} \right) + 1 \right] \quad (5)$$

where V_{rev} (V) is the reversible voltage, the second term is the ohmic overvoltage defined by its parameter r (Ω m^2) and the last term represents the activation overvoltage defined by the parameters s (V) and t (m^2 A^{-1}). The current absorbed by the electrolyzer is represented by i_{el} (A), while A_{elec} (m^2) stands for the cell electrode area. The term i_{el}/A_{elec} (A m^{-2}) is the current density that can be replaced by j (A m^{-2}).

Based on the article Ref. [30], the performance of the alkaline electrolyzer highly depends on its operating temperature. Therefore, to improve the above semi-empirical model, the temperature effect must be considered. As reported in Ref. [31], only the two parameters r and t depend on the temperature while the parameter s is usually assumed to be constant. Considering the electrolyzer operating temperature, Ulleberg's model in Equation (5) can be modified as expressed in the following Equation (6):

$$V_{cell} = V_{rev} + \left(r_1 + r_2 \cdot \theta\right) \cdot j + s \cdot \log\left[\left(t_1 + \frac{t_2}{\theta} + \frac{t_3}{\theta^2} \right) \cdot j + 1 \right] \quad (6)$$

where θ (°C) is the operating temperature, r_1 (Ω m^2) and r_2 (Ω m^2 °C^{-1}) reflect ohmic losses, t_1 (m^2 A^{-1}), t_2 (m^2 A^{-1} °C) and t_3 (m^2 A^{-1} °C^2) are related to the activation over voltages and j (A m^{-2}) is the current density [18].

Gas pressure also influences the performance of the alkaline electrolyzer [18,30]. Also considering the gas pressure P (bar), the above Ulleberg's equation can be expressed in Equation (7) as:

$$V_{cell} = V_{rev} + \left[\left(r_1 + \delta_1\right) + r_2 \cdot \theta + \delta_2 \cdot P\right] \cdot j + s \cdot \log\left[\left(t_1 + \frac{t_2}{\theta} + \frac{t_3}{\theta^2} \right) \cdot j + 1 \right] \quad (7)$$

Equation (7) introduces new empirical parameters δ_1 (Ω m^2) and δ_2 (Ω m^2 bar^{-1}), which are related to the linear change in the ohmic overvoltage.

Many authors have demonstrated that the distance electrode-diaphragm d (mm) [32] and the electrolyte molarity concentration M (mol l^{-1}) have a significant influence on the alkaline electrolyzer performances. The ohmic losses depend on the electrode-diaphragm distance d and the electrolyte molarity concentration M. To obtain an accurate equation for the current-voltage curve, these two new parameters must be examined. Thus, the resulting semi-empirical model is given by Equation (8) below:

$$V_{cell} = V_{rev} + \left[\left(r_1 + p_1 + q_1\right) + r_2 \cdot \theta + p_2 M + p_3 M^2 + q_2 \cdot d\right] \cdot j + s \cdot \log\left[\left(t_1 + \frac{t_2}{\theta} + \frac{t_3}{\theta^2} \right) \cdot j + 1 \right] \quad (8)$$

where p_1 (Ω m^2), p_2 (Ω m^2 mol^{-1} l), and p_3 (Ω m^2 mol^{-2} l^2) represent the ohmic drops due to the electrolyte concentration, q_1 (Ω m^2) and q_2 (Ω m^2 mm^{-1}) represent the ohmic losses due to the electrode-diaphragm distance.

To determine the different parameters in Equations (6)-(8), experimental data are compared to the model through the use of a numerical regression method mainly based on least square algorithms [33–35]. Relying on previous works carried out to determine the parameters of the models (6)-(8), Table 4 has been made to summarize the values of the different parameters.

Finally, considering that all the cells in the alkaline electrolyzer have the same physical performance and behavior, then the electrolyzer total voltage (V_{el}) is equal to the cell voltage (V_{cell}) multiplied by the number of cells of the stack N_{cell} as reported in Equation (9) below:

$$V_{el} = N_{cell} \cdot V_{cell} \quad (9)$$

In the next subsection, empirical models are reported and detailed.

Table 4. Parameters for the calculation of the cell voltage for Equation (6), (7) and (8).

Parameter	Equation (6) [18,29]	Equation (7) [18,30]	Equation (8) [32]	Unit
r_1	$8.05.10^{-5}$	$4.45153.10^{-5}$	$3.53855.10^{-4}$	$\Omega\ m^2$
r_2	$-2.5.10^{-7}$	$6.88874.10^{-9}$	$-3.02150.10^{-6}$	$\Omega\ m^2\ °C^{-1}$
s	0.185	0.33824	$2.2396.10^{-1}$	V
t_1	1.002	-0.01539	5.13093	$m^2\ A^{-1}$
t_2	8.424	2.00181	$-2.40447.10^{2}$	$m^2\ °C\ A^{-1}$
t_3	247.3	15.24178	$5.99576.10^{3}$	$m^2\ °C^2\ A^{-1}$
δ_1	-	$-3.12996.10^{-6}$	-	$\Omega\ m^2$
δ_2	-	$4.47137.10^{-7}$	-	$\Omega\ m^2\ bar^{-1}$
p_1	-	-	$3.410251.10^{-4}$	$\Omega\ m^2$
p_2	-	-	$-7.489577.10^{-5}$	$\Omega\ m^2\ mol^{-1}\ l$
p_3	-	-	$3.916035.10^{-6}$	$\Omega\ m^2\ mol^{-2}\ l^2$
q_1	-	-	$-1.576117.10^{-4}$	$\Omega\ m^2$
q_2	-	-	$1.576117.10^{-5}$	$\Omega\ m^2\ mm^{-1}$

3.1.3. Empirical modeling

As reported in the literature, the main electrical expression of the cell voltage V_{cell} including the different voltages is given by Equation (10) [18,36]:

$$V_{cell} = V_{rev} + \left(R_a + R_c + R_{ele} + R_{mem}\right) \cdot i_{el} + \eta_{act,a} + \eta_{act,c} \quad (10)$$

where V_{rev} (V) is the reversible voltage, R_a (Ω) and R_c (Ω) are ohmic resistances respectively related to the conductivity of the electrodes (anode and cathode), R_{ele} (Ω) represents the ohmic loss due to the electrolyte conductivity, R_{mem} (Ω) stands for the membrane ohmic resistance, $\eta_{act,a}$ (V) and $\eta_{act,c}$ (V) are respectively the activation overvoltage at the anode and the cathode.

In this subsection, the expressions of the reversible voltage and the different overvoltages (activation and ohmic) are provided and studied.

Reversible potential

The reversible potential is defined as a required voltage that is just needed to start the electrolysis reaction. Its value is directly related to the Gibbs energy ΔG (J mol^{-1}) defined in Equation (11) below [15,18,29]:

$$\Delta G = \Delta H - T \cdot \Delta S \quad (11)$$

where ΔH (J mol^{-1}) is the change in enthalpy, ΔS (J mol^{-1} °K^{-1}) the change in entropy and T (°K) the temperature.

The reversible potential V_{rev} is the ratio of the Gibbs energy ΔG to the product of Faraday's constant F and the number of exchanged electrons n, as given in Equation (12) below:

$$V_{rev} = \frac{\Delta G}{n \cdot F} = \frac{\Delta H - T \cdot \Delta S}{n \cdot F} \quad (12)$$

The change in enthalpy ΔH is also related to the thermoneutral cell voltage V_{th} by the following Equation (13):

$$V_{th} = \frac{\Delta H}{n \cdot F} = \frac{\Delta G + T \cdot \Delta S}{n \cdot F} \quad (13)$$

Given that the number of electrons n = 2 (see chemical reactions, Equations (1-3)) and the Faraday's constant F = 96,485 C mol^{-1}, at standard conditions (T= 298.15 °K, pressure of 1 bar), the values of the enthalpy ΔH and the entropy ΔS are given as: ΔH=285.84 kJ mol^{-1}, ΔS=0.1631 kJ mol^{-1} °K^{-1}. At these conditions, the reversible potential and the thermoneutral cell voltage are respectively given by: $V_{rev,0}$ = 1.23 V and $V_{th,0}$ = 1.48 V.

At other operating conditions, the reversible potential V_{rev} (V) is determined using Nernst's equation in Equation (14) as reported in articles [32,37,38]:

$$V_{rev} = V_{rev,0,T} + \frac{R \cdot T}{n \cdot F} \cdot \ln\left(\frac{\left(P - P_{v,KOH}\right)^{3/2}}{\alpha_{H_2O}} \right) \quad (14)$$

where $V_{rev,0,T}$ (V) is the reversible potential at a given condition (i.e. temperature and pressure), R = 8.315 J K^{-1} mol^{-1} the universal gas constant, T (°K) the temperature, n the number of electrons, F (C mol^{-1}) the Faraday's constant, P (bar) the gas pressure, $P_{v,KOH}$ (bar) the vapor pressures, and α_{H2O} is the water activity of the electrolyte solution based on KOH.

The reversible potential $V_{rev,0,T}$ (V) can be assessed as a function of temperature T (°K) in Equation (15) as reported in articles [37–40]:

$$V_{rev,0,T} = 1.5184 - 1.5421 \cdot 10^{-3} \cdot T + 9.523 \cdot 10^{-5} \cdot T \cdot \ln(T) + 9.84 \cdot 10^{-8} \cdot T^2 \quad (15)$$

The vapor pressures of the KOH solution $P_{v,KOH}$ (bar) is calculated using the following Equation (16) as reported in [37]:

$$P_{v,KOH} = \exp\left(2.302 \cdot a + b \cdot \ln\left(P_{v,H_2O}\right)\right) \quad (16)$$

where a and b are coefficients that depend on the KOH molality m (mol kg^{-1}) as given in Equations (17) and (18) below, and $P_{v,H2O}$ (bar) is the vapor pressure of pure water which is expressed as a function of the temperature T (°K) in Equation (19) as reported in [37]:

$$a = -0.0151 \cdot m - 1.6788 \cdot 10^{-3} \cdot m^2 + 2.2588 \cdot 10^{-5} \cdot m^3 \quad (17)$$

$$b = 1 - 1.2062 \cdot 10^{-3} \cdot m + 5.6024 \cdot 10^{-4} \cdot m^2 - 7.8228 \cdot 10^{-6} \cdot m^3 \quad (18)$$

$$P_{v,H_2O} = \exp\left(81.6179 - \frac{7699.68}{T} - 10.9 \cdot \ln T + 9.5891 \cdot 10^{-3} \cdot T\right) \quad (19)$$

In Equation (20), the water activity α_{H2O} of the electrolyte solution based on KOH is expressed as a function of the temperature T (°K) and the molality concentration m (mol kg^{-1}) as reported in [37]:

$$\alpha_{H_2O} = \exp\left(-0.05192 \cdot m + 0.003302 \cdot m^2 + \frac{\left(3.177 \cdot m - 2.131 \cdot m^2\right)}{T}\right) \quad (20)$$

Equations (15)-(20) are valid for pressure ranging from 1 to 200 bar, temperature between 273.15 to 523.15 °K, and the molality concentration ranging from 2 to 18 mol kg^{-1}.

Activation overpotential

The activation overvoltages starting the water electrolysis process at the anode $\eta_{act,a}$ and at the cathode $\eta_{act,c}$ can be evaluated using the Butler–Volmer equations (or Tafel's approximations) in Equations (21) and (22) as reported in articles [36,39].

$$\eta_{act,a} = 2.3 \cdot \frac{R \cdot T}{\alpha_a \cdot F} \cdot \log\left(\frac{j_a}{j_{0,a}}\right) \quad (21)$$

$$\eta_{act,c} = 2.3 \cdot \frac{R \cdot T}{\alpha_c \cdot F} \cdot \log\left(\frac{j_c}{j_{0,c}}\right) \quad (22)$$

where α_a and α_c are respectively the charge transfer coefficients at the anode and the cathode, j_a (mA cm^{-2}) and j_c (mA cm^{-2}) are the current densities of the electrodes, $j_{0,a}$ (mA cm^{-2}) and $j_{0,c}$ (mA cm^{-2}) are the exchange current densities of the electrodes.

Based on the physical and electrical behavior of the Hydrogen Research Institute (HRI) alkaline electrolyzer reported in [36], the physical models of the current densities ($j_{0,a}$ and $j_{0,c}$) as a function of temperature T (°K) are given in Equations (23) and (24):

$$j_{0,a} = 30.4 - 0.206 \cdot T + 0.00035 \cdot T^2 \quad (23)$$

$$j_{0,c} = 13.72491 - 0.09055 \cdot T + 0.09055 \cdot T^2 \quad (24)$$

The charge transfer coefficients (α_a and α_c) of the HRI electrolyser as a function of temperature T (°K) are given in Equations (25) and (26) as reported in [36]:

$$\alpha_a = 0.0675 + 0.00095 \cdot T \quad (25)$$

$$\alpha_c = 0.1175 + 0.00095 \cdot T \quad (26)$$

Ohmic overpotential

Alkaline electrolyzers are made of different elements. Each element is modeled as electrical resistance. The total ohmic resistance of the electrolyzer can be expressed in Equation (27) as reported in articles [36,41]:

$$R_{total} = R_a + R_c + R_{ele} + R_{mem} \quad (27)$$

where R_a (Ω) and R_c (Ω) are the anode and the cathode resistances, R_{ele} (Ω) the resistance of the electrolyte (KOH or NaOH), and R_{mem} (Ω) the resistance of the membrane.

a) Electrodes

Electrodes in alkaline electrolyzer can either be cobalt, nickel, or iron. Most of the electrodes are made of nickel because of their stability [9]. Electrodes resistances depend on their conductivity and their geometry as reported in the article [36]. Therefore, the resistances at the anode R_a and the cathode R_c of electrodes made of nickel (Ni) are given in Equations (28) and (29) as reported in [36] :

$$R_a = \frac{1}{\sigma_{Ni}}\left(\frac{L_a}{S_a}\right) \quad (28)$$

$$R_c = \frac{1}{\sigma_{Ni}}\left(\frac{L_c}{S_c}\right) \quad (29)$$

where L_a (cm) and L_c (cm) are respectively the anode and the cathode thicknesses, S_a (cm²) and S_c (cm²) are the electrodes cross sections, and σ_{Ni} (S cm^{-1}) is the conductivity of an electrode made of nickel.

As reported in the article [36], the conductivity σ_{Ni} can be calculated as a function of temperature T (°K) using the following Equation (30):

$$\sigma_{Ni} = 6000000 - 279650 \cdot T + 532 \cdot T^2 - 0.38057 \cdot T^3 \quad (30)$$

b) Electrolytes

The alkaline electrolysis reaction generates bubbles from hydrogen and oxygen gases, thus the electrolyte resistance R_{ele} in Equation (31) is the sum of the bubble-free electrolyte resistance $R_{ele,bf}$ and the resistance due to bubbles $R_{ele,b}$ as reported in articles [36,42]:

$$R_{ele} = R_{ele,bf} + R_{ele,b} \quad (31)$$

In articles [36,42], the formula used to calculate the bubble-free electrolyte resistance $R_{ele,bf}$ is given in Equation (32) below:

$$R_{ele,bf} = \frac{1}{\sigma_{bf}}\left(\frac{d_{a,m}}{S_a} + \frac{d_{c,m}}{S_c}\right) \quad (32)$$

where $d_{a,m}$ (cm) and $d_{c,m}$ (cm) are respectively the anode-membrane and the cathode-membrane distances, S_a (cm²) and S_c (cm²) are the anode and cathode cross-sections and σ_{bf} (S m^{-1}) is the bubble-free electrolyte conductivity.

The bubble-free conductivity σ_{bf} can be determined as a function of the electrolyte molarity concentration M (mol l^{-1}) and the temperature T (°K) as reported in [36,39,43] according to Equation (33) below:

$$\sigma_{bf} = -204.1 \cdot M - 0.28 \cdot M^2 + 0.5332 \cdot (M \cdot T) + 20720 \cdot \frac{M}{T} + 0.1043 \cdot M^3 - 0.00003 \cdot (M^2 \cdot T^2) \quad (33)$$

The equation (33) can also be expressed according to the temperature and KOH mass fractions. Since it is an important issue in this review paper, it is analyzed and detailed in the next subsection.

The resistance $R_{ele,b}$ due to bubbles in the electrolyte is given in Equation (34) as reported in the article [36]:

$$R_{ele,b} = R_{ele,bf} \cdot \left(\frac{1}{(1-\varepsilon)^{3/2}} - 1 \right) \quad (34)$$

where ε is a coefficient that depends on the effective electrode surface S_{eff} (cm²) and the nominal electrode surface S (cm²) as given in Equation (35):

$$\varepsilon = 1 - \left(\frac{S_{eff}}{S} \right) \quad (35)$$

c) Membrane

As reported in [36], the HRI electrolyzer membrane resistance made of Zirfon material of 0.5 mm thickness is given in Equation (36) as:

$$R_{mem} = \frac{0.060 + 80 \cdot \exp(T/50)}{10000 \cdot S_{mem}} \quad (36)$$

where S_{mem} (cm²) is the membrane surface, T (°K) is the temperature.

After analyzing the semi-empirical and empirical models, the next subsection allows introducing the dynamic modeling of alkaline electrolyzers that has to be considered when coupling them with intermittent energy sources.

3.2. Dynamic modeling

Compared to static modeling, dynamic modeling of alkaline electrolyzers has received fewer investigations from researchers. Indeed, over the last decade, only two papers have considered dynamic issues when modeling alkaline electrolyzers [37,44]. First of all, in [37], the authors have proposed an equivalent electrical circuit to model both static and dynamic behaviors of this electrolyzer. This equivalent electrical circuit for one cell is shown in Figure 7. It is composed of the following components linked to the previous analysis reported in this section:

1. A DC source, V_{rev}, represents the reversible voltage (located on the cathode side where the hydrogen is generated).
2. A current source ($i_{act,a}$ or $i_{act,c}$) connected in parallel with a capacitor C_a or C_C modeling the activation overvoltage and especially the well-known double-layer effect between the electrode (anode or cathode) and the electrolyte.
3. Four resistors R_a, R_c, R_{mem}, and R_{ele} model respectively the anode, cathode, membrane, and electrolyte.

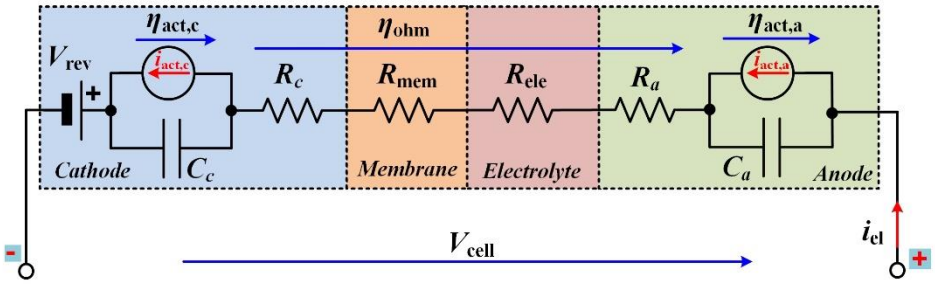

Figure 7. Equivalent electrical circuit modeling both static and dynamic behaviors for one cell.

Both current sources ($i_{act,a}$ and $i_{act,c}$) of the electrical circuit enable replicating the activation phenomena for the anode and the cathode. These sources can be modeled as a function of their activation overvoltages ($\eta_{act,a}$ and $\eta_{act,c}$), relying on a fit Tafel expression provided below valid for the whole stack of the electrolyzer [37]:

$$\eta_{act,a,el} = N_{cell} \cdot \eta_{act,a} = s_a \cdot \log\left[t_a \cdot \left(\frac{i_{act,a}}{A_{elec,a}}\right) + 1\right] \Rightarrow i_{act,a} = \frac{A_{elec,a}}{t_a} \cdot \left[10^{\left(\frac{\eta_{act,a,el}}{s_a \cdot N_{cell}}\right)} - 1\right] \quad (37)$$

$$\eta_{act,c,el} = N_{cell} \cdot \eta_{act,c} = s_c \cdot \log\left[t_c \cdot \left(\frac{i_{act,c}}{A_{elec,c}}\right) + 1\right] \Rightarrow i_{act,c} = \frac{A_{elec,c}}{t_c} \cdot \left[10^{\left(\frac{\eta_{act,c,el}}{s_c \cdot N_{cell}}\right)} - 1\right] \quad (38)$$

where

$$t_a = t_{a1} + \frac{t_{a2}}{\theta} + \frac{t_{a3}}{\theta^2} \quad (39)$$

$$t_c = t_{c1} + \frac{t_{c2}}{\theta} + \frac{t_{c3}}{\theta^2} \quad (40)$$

The equivalent electrical circuit (Figure 7) can be simplified as depicted in Figure 8 [44]. In this circuit, the activation branch at the cathode side ($i_{act,c}$ and C_C) has been neglected since its overpotential is lower than the overpotential at the anode side [15]. Besides, in [44], a first value of the capacitance has been provided, equal to 15 mF. This value is much lower than those reported for PEM electrolyzers [45]. Indeed, for PEM electrolyzers, capacitance values from 3 to 69 F have been reported according to the operating conditions. Based on the dynamic tests provided in Figures 4 and 5, alkaline electrolyzers can respond quickly to sudden operating conditions changes. This analysis can explain the small value of the capacitance for this electrolyzer technology, whereas for PEM electrolyzers, the dynamics met are more meaningful. Hence, the values of capacitance are higher than alkaline electrolyzers.

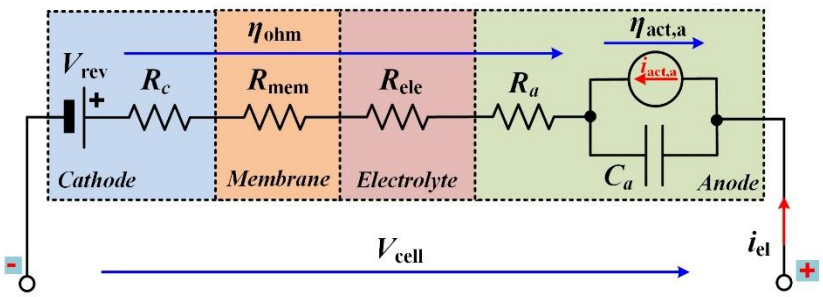

Figure 8. Simplified equivalent electrical circuit modeling both static and dynamic behaviors for one cell.

3.3. Specific electrolyte conductivity

The specific electrolyte conductivity for KOH and NaOH are given in Equation (41) and (42). Equations (41) is valid for temperature T (°K) ranging from 258.15 to 373.15°K and KOH mass fraction w_{KOH} between 0.15 and 0.45, while Equation (42) is suitable for temperatures θ (°C) between 25 and 50 °C and NaOH mass fraction w_{NaOH} from 0.08 to 0.25 as reported in the article [18]. The parameters needed to calculate these conductivities are listed in Table 5.

$$\sigma_{KOH} = K_1 \cdot (100 \cdot w_{KOH}) + K_2 \cdot T + K_3 \cdot T^2 + K_4 \cdot T \cdot (100 \cdot w_{KOH}) + K_5 \cdot T^2 \cdot (100 \cdot w_{KOH})^{K_6} + K_7 \cdot \frac{T}{(100 \cdot w_{KOH})} + K_8 \cdot \frac{(100 \cdot w_{KOH})}{T} \quad (41)$$

$$\sigma_{NaOH} = K_1 + K_2 \cdot \theta + K_3 \cdot w_{NaOH}^3 + K_4 \cdot w_{NaOH}^2 + K_5 \cdot w_{NaOH} \quad (42)$$

Table 5. Parameters for the calculation of the specific electrolyte conductivities of KOH and NaOH solutions by Equations (41) and (42)[18].

Parameter	Equation (41)	Unit	Equation (42)	Unit
K_1	27.984 480 3	$S\ m^{-1}$	-45.7	$S\ m^{-1}$
K_2	-0.924 129 482	$S\ m^{-1}\ K^{-1}$	1.02	$S\ m^{-1}\ °C^{-1}$
K_3	-0.014 966 037 1	$S\ m^{-1}\ K^{-2}$	3200	$S\ m^{-1}$
K_4	-0.090 520 955 1	$S\ m^{-1}\ K^{-1}$	-2990	$S\ m^{-1}$
K_5	0.011 493 325 2	$S\ m^{-1}\ K^{-2}$	784	$S\ m^{-1}$
K_6	0.1765	-	-	-
K_7	6.966 485 18	$S\ m^{-1}\ K^{-1}$	-	-
K_8	-2898.156 58	$S\ m^{-1}\ K$	-	-

Relying on the equations (41)-(42) and the parameters of both equations reported in Table 5, the specific electrolyte conductivity of KOH and NaOH has been plotted according to the mass fraction w as shown in Figure 9. Besides, two temperatures have been considered, 25 and 50°C.

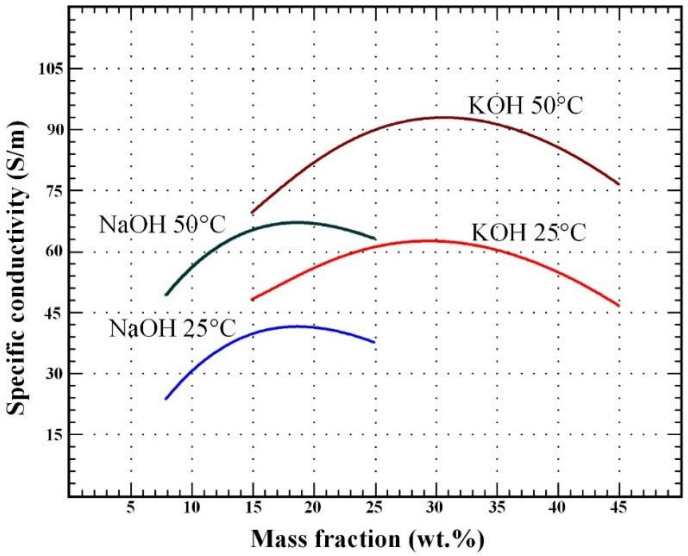

Figure 9. Specific electrolyte conductivity for liquid solutions based on either KOH or NaOH according to the mass fraction of the solution.

Based on Figure 9, one can note that for alkaline electrolyzers with KOH liquid solution, the specific electrolyte conductivity is higher compared to alkaline electrolyzers with NaOH solution. Indeed, as it has been demonstrated in previous papers [18,42], the specific electrolyte conductivity of KOH is optimal for mass fractions between 25 and 35 wt.% and a temperature range from 50 to 80°C. The use of a liquid solution based on NaOH offers a cheaper option than KOH but features a lower specific electrolyte conductivity. For example, at 50°C, the maximum specific electrolyte conductivity of KOH is equal to 95 $S.m^{-1}$, whereas for NaOH the conductivity is equal to 65 $S.m^{-1}$. By comparison, at 25°C, both specific electrolyte conductivities have decreased, 63 $S.m^{-1}$ for KOH and 42 $S.m^{-1}$ for NaOH. Furthermore, it is important to point out that the specific electrolyte conductivity of NaOH is optimal for lower mass fractions between 15 and 25 wt.% and temperatures between 50 and 80°C. In summary, KOH liquid solution features a specific electrolyte conductivity between 46 and 50% higher than NaOH liquid solution at their optimal mass fractions.

4. Conclusions

The purpose of this paper was to review the modeling of alkaline electrolyzers from the electrical domain and specific electrolyte conductivity points of view. It has been emphasized that modeling of this electrolyzer technology has received less interest from researchers compared to PEM electrolyzers. However, alkaline electrolyzers feature several benefits in terms of cost due to cheaper catalysts, high lifespan, gas purity, hydrogen production capacity, and low specific energy consumption. However, this technology still suffers from having limited current density and production capacity range and requesting frequent maintenance due to the use of an aqueous electrolyte solution. Since this technology is quite mature, several perspectives are considered such as the increase in the use of non-precious metals combined with nickel material to enhance the performance, the design in spacing electrodes to optimize hydrogen production, and the dissemination of low carbon footprint hydrogen production plants supplied by renewable and nuclear resources. Besides, as demonstrated in this paper, alkaline electrolyzers can respond quickly to dynamic solicitations and are consequently suitable to be coupled with renewable energy sources such as wind turbine conversion systems. The literature review focused on the electrical domain modeling has enabled to bring out the lacks. Indeed, static modeling has been widely investigated, but dynamic modeling has not been thoroughly analyzed. Hence, further research investigations are requested to bring new knowledge of alkaline electrolyzer's behaviors supplied by dynamic sources and the modeling of these behaviors through the development of equivalent electrical circuits.

Author Contributions: conceptualization, F.G., D.G., M.Z., and H.R.; methodology, F.G., D.G.; validation, F.G. and D.G.; investigation, F.G. and D.G.; writing—original draft preparation, F.G., D.G.; writing—review and editing, F.G., D.G. All authors have read and agreed to the published version of the manuscript.

Funding: The experimental hydrogen platform presented in this paper has been realized thanks to the financial support of the IUT of Longwy, CRAN, and GREEN research laboratories.

Acknowledgments: The authors would like to express their gratitude to the IUT of Longwy, CRAN, and GREEN research laboratories for their constant support in developing fruitful cooperation between CRAN and GREEN research teams from the IUT de Longwy campus.

Conflicts of Interest: The authors declare no conflict of interest.

References

1. Shiva Kumar, S.; Himabindu, V. Hydrogen Production by PEM Water Electrolysis – A Review. *Materials Science for Energy Technologies* **2019**, *2*, 442–454, doi:10.1016/j.mset.2019.03.002.
2. Carmo, M.; Fritz, D.L.; Mergel, J.; Stolten, D. A Comprehensive Review on PEM Water Electrolysis. *International Journal of Hydrogen Energy* **2013**, *38*, 4901–4934, doi:10.1016/j.ijhydene.2013.01.151.
3. Falcão, D.S.; Pinto, A.M.F.R. A Review on PEM Electrolyzer Modelling: Guidelines for Beginners. *Journal of Cleaner Production* **2020**, *261*, 121184, doi:10.1016/j.jclepro.2020.121184.
4. Buttler, A.; Spliethoff, H. Current Status of Water Electrolysis for Energy Storage, Grid Balancing and Sector Coupling via Power-to-Gas and Power-to-Liquids: A Review. *Renewable and Sustainable Energy Reviews* **2018**, *82*, 2440–2454, doi:10.1016/j.rser.2017.09.003.
5. Apostolou, D. Optimisation of a Hydrogen Production – Storage – Re-Powering System Participating in Electricity and Transportation Markets. A Case Study for Denmark. *Applied Energy* **2020**, *265*, 114800, doi:10.1016/j.apenergy.2020.114800.
6. Guilbert, D.; Vitale, G. Hydrogen as a Clean and Sustainable Energy Vector for Global Transition from Fossil-Based to Zero-Carbon. *Clean Technologies* **2021**, *3*, 881–909, doi:10.3390/cleantechnol3040051.
7. Https://Ec.Europa.Eu/Growth/Industry/Strategy/Hydrogen_en.
8. Yodwong, B.; Guilbert, D.; Phattanasak, M.; Kaewmanee, W.; Hinaje, M.; Vitale, G. AC-DC Converters for Electrolyzer Applications: State of the Art and Future Challenges. *Electronics* **2020**, *9*, 912, doi:10.3390/electronics9060912.
9. David, M.; Ocampo-Martínez, C.; Sánchez-Peña, R. Advances in Alkaline Water Electrolyzers: A Review. *Journal of Energy Storage* **2019**, *23*, 392–403, doi:10.1016/j.est.2019.03.001.
10. Li, C.; Baek, J.-B. The Promise of Hydrogen Production from Alkaline Anion Exchange Membrane Electrolyzers. *Nano Energy* **2021**, *87*, 106162, doi:10.1016/j.nanoen.2021.106162.
11. Carmo, M.; Stolten, D. Chapter 4 - Energy Storage Using Hydrogen Produced From Excess Renewable Electricity: Power to Hydrogen. In *Science and Engineering of Hydrogen-Based Energy Technologies*; de Miranda, P.E.V., Ed.; Academic Press, 2019; pp. 165–199 ISBN 978-0-12-814251-6.
12. Wulf, C.; Linssen, J.; Zapp, P. Chapter 9 - Power-to-Gas—Concepts, Demonstration, and Prospects. In *Hydrogen Supply Chains*; Azzaro-Pantel, C., Ed.; Academic Press, 2018; pp. 309–345 ISBN 978-0-12-811197-0.
13. *PEM Electrolysis for Hydrogen Production: Principles and Applications*; Bessarabov, D., Wang, H., Li, H., Zhao, N., Eds.; CRC Press: Boca Raton, 2015; ISBN 978-0-429-18360-7.
14. Schalenbach, M.; Carmo, M.; Fritz, D.L.; Mergel, J.; Stolten, D. Pressurized PEM Water Electrolysis: Efficiency and Gas Crossover. *International Journal of Hydrogen Energy* **2013**, *38*, 14921–14933, doi:10.1016/j.ijhydene.2013.09.013.
15. Hernández-Gómez, Á.; Ramirez, V.; Guilbert, D. Investigation of PEM Electrolyzer Modeling: Electrical Domain, Efficiency, and Specific Energy Consumption. *International Journal of Hydrogen Energy* **2020**, *45*, 14625–14639, doi:10.1016/j.ijhydene.2020.03.195.
16. Yodwong, B.; Guilbert, D.; Phattanasak, M.; Kaewmanee, W.; Hinaje, M.; Vitale, G. Proton Exchange Membrane Electrolyzer Modeling for Power Electronics Control: A Short Review. *C* **2020**, *6*, 29, doi:10.3390/c6020029.
17. Millet, P.; Ranjbari, A.; de Guglielmo, F.; Grigoriev, S.A.; Auprêtre, F. Cell Failure Mechanisms in PEM Water Electrolyzers. *International Journal of Hydrogen Energy* **2012**, *37*, 17478–17487, doi:10.1016/j.ijhydene.2012.06.017.

18. Brauns, J.; Turek, T. Alkaline Water Electrolysis Powered by Renewable Energy: A Review. *Processes* **2020**, *8*, 248, doi:10.3390/pr8020248.
19. Shirvanian, P.; Loh, A.; Sluijter, S.; Li, X. Novel Components in Anion Exchange Membrane Water Electrolyzers (AEMWE's): Status, Challenges and Future Needs. A Mini Review. *Electrochemistry Communications* **2021**, *132*, 107140, doi:10.1016/j.elecom.2021.107140.
20. Wang, L.; Chen, M.; Küngas, R.; Lin, T.-E.; Diethelm, S.; Maréchal, F.; Van herle, J. Power-to-Fuels via Solid-Oxide Electrolyzer: Operating Window and Techno-Economics. *Renewable and Sustainable Energy Reviews* **2019**, *110*, 174–187, doi:10.1016/j.rser.2019.04.071.
21. Demo4Grid Project, Https://Www.Demo4grid.Eu/ (Accessed Jan 11, 2022).
22. CEOG Project | McPhy Https://Mcphy.Com/En/Press-Releases/Ceog-Project/?Cn-Reloaded=1 (Accessed Jan 11, 2022).
23. Roventi, G.; Cecchini, R.; Fabrizi, A.; Bellezze, T. Electrodeposition of Nickel–Zinc Alloy Coatings with High Nickel Content. *Surface and Coatings Technology* **2015**, *276*, 1–7, doi:10.1016/j.surfcoat.2015.06.043.
24. Okonkwo, P.C.; Bhowmik, H.; Mansir, I.B.; Al Sarj Al Marhoon, M.A.A.; Al Sfarini, N.F.A. Effect of Electrode Spacing on Hydrogen Production Using a Home-Made Alkaline Electrolyzer. *Materials Letters* **2022**, *306*, 130841, doi:10.1016/j.matlet.2021.130841.
25. Yue, M.; Lambert, H.; Pahon, E.; Roche, R.; Jemei, S.; Hissel, D. Hydrogen Energy Systems: A Critical Review of Technologies, Applications, Trends and Challenges. *Renewable and Sustainable Energy Reviews* **2021**, *146*, 111180, doi:10.1016/j.rser.2021.111180.
26. Keddar, M.; Zhang, Z.; Periasamy, C.; Doumbia, M.L. Comparative Analysis of Thyristor-Based and Transistor-Based Rectifiers for PEM Water Electrolysis. In Proceedings of the 2021 12th International Renewable Energy Congress (IREC); October 2021; pp. 1–5.
27. Koponen, J.; Poluektov, A.; Ruuskanen, V.; Kosonen, A.; Niemelä, M.; Ahola, J. Comparison of Thyristor and Insulated-Gate Bipolar Transistor -Based Power Supply Topologies in Industrial Water Electrolysis Applications. *Journal of Power Sources* **2021**, *491*, 229443, doi:10.1016/j.jpowsour.2020.229443.
28. Brauns, J.; Turek, T. Experimental Evaluation of Dynamic Operating Concepts for Alkaline Water Electrolyzers Powered by Renewable Energy. *Electrochimica Acta* **2022**, *404*, 139715, doi:10.1016/j.electacta.2021.139715.
29. Ulleberg, Ø. Modeling of Advanced Alkaline Electrolyzers: A System Simulation Approach. *International Journal of Hydrogen Energy* **2003**, *28*, 21–33, doi:10.1016/S0360-3199(02)00033-2.
30. Sánchez, M.; Amores, E.; Rodríguez, L.; Clemente-Jul, C. Semi-Empirical Model and Experimental Validation for the Performance Evaluation of a 15 KW Alkaline Water Electrolyzer. *International Journal of Hydrogen Energy* **2018**, *43*, 20332–20345, doi:10.1016/j.ijhydene.2018.09.029.
31. Ursúa, A.; San Martín, I.; Barrios, E.L.; Sanchis, P. Stand-Alone Operation of an Alkaline Water Electrolyser Fed by Wind and Photovoltaic Systems. *International Journal of Hydrogen Energy* **2013**, *38*, 14952–14967, doi:10.1016/j.ijhydene.2013.09.085.
32. Amores, E.; Rodríguez, J.; Carreras, C. Influence of Operation Parameters in the Modeling of Alkaline Water Electrolyzers for Hydrogen Production. *International Journal of Hydrogen Energy* **2014**, *39*, 13063–13078, doi:10.1016/j.ijhydene.2014.07.001.
33. Ma, Z.; Witteman, L.; Wrubel, J.A.; Bender, G. A Comprehensive Modeling Method for Proton Exchange Membrane Electrolyzer Development. *International Journal of Hydrogen Energy* **2021**, *46*, 17627–17643, doi:10.1016/j.ijhydene.2021.02.170.

34. David, M.; Alvarez, H.; Ocampo-Martinez, C.; Sánchez-Peña, R. Dynamic Modelling of Alkaline Self-Pressurized Electrolyzers: A Phenomenological-Based Semiphysical Approach. *International Journal of Hydrogen Energy* **2020**, *45*, 22394–22407, doi:10.1016/j.ijhydene.2020.06.038.
35. Ruuskanen, V.; Koponen, J.; Huoman, K.; Kosonen, A.; Niemelä, M.; Ahola, J. PEM Water Electrolyzer Model for a Power-Hardware-in-Loop Simulator. *International Journal of Hydrogen Energy* **2017**, *42*, 10775–10784, doi:10.1016/j.ijhydene.2017.03.046.
36. Henao, C.; Agbossou, K.; Hammoudi, M.; Dubé, Y.; Cardenas, A. Simulation Tool Based on a Physics Model and an Electrical Analogy for an Alkaline Electrolyser. *Journal of Power Sources* **2014**, *250*, 58–67, doi:10.1016/j.jpowsour.2013.10.086.
37. Ursúa, A.; Sanchis, P. Static–Dynamic Modelling of the Electrical Behaviour of a Commercial Advanced Alkaline Water Electrolyser. *International Journal of Hydrogen Energy* **2012**, *37*, 18598–18614, doi:10.1016/j.ijhydene.2012.09.125.
38. Adibi, T.; Sojoudi, A.; Saha, S.C. Modeling of Thermal Performance of a Commercial Alkaline Electrolyzer Supplied with Various Electrical Currents. *International Journal of Thermofluids* **2022**, *13*, 100126, doi:10.1016/j.ijft.2021.100126.
39. Rodríguez, J.; Amores, E. CFD Modeling and Experimental Validation of an Alkaline Water Electrolysis Cell for Hydrogen Production. *Processes* **2020**, *8*, 1634, doi:10.3390/pr8121634.
40. Janjua, M.B.I.; Le Roy, R.L. Electrocatalyst Performance in Industrial Water Electrolysers. *International Journal of Hydrogen Energy* **1985**, *10*, 11–19, doi:10.1016/0360-3199(85)90130-2.
41. Lavorante, M.J.; Franco, J. Performance of Stainless Steel 316L Electrodes with Modified Surface to Be Use in Alkaline Water Electrolyzers. **2016**, doi:10.1016/J.IJHYDENE.2016.02.096.
42. Brauns, J.; Schönebeck, J.; Kraglund, M.R.; Aili, D.; Hnát, J.; Žitka, J.; Mues, W.; Jensen, J.O.; Bouzek, K.; Turek, T. Evaluation of Diaphragms and Membranes as Separators for Alkaline Water Electrolysis. *J. Electrochem. Soc.* **2021**, *168*, 014510, doi:10.1149/1945-7111/abda57.
43. Gilliam, R.J.; Graydon, J.W.; Kirk, D.W.; Thorpe, S.J. A Review of Specific Conductivities of Potassium Hydroxide Solutions for Various Concentrations and Temperatures. *International Journal of Hydrogen Energy* **2007**, *32*, 359–364, doi:10.1016/j.ijhydene.2006.10.062.
44. Speckmann, F.-W.; Bintz, S.; Birke, K.P. Influence of Rectifiers on the Energy Demand and Gas Quality of Alkaline Electrolysis Systems in Dynamic Operation. *Applied Energy* **2019**, *250*, 855–863, doi:10.1016/j.apenergy.2019.05.014.
45. Hernández-Gómez, Á.; Ramirez, V.; Guilbert, D.; Saldivar, B. Self-Discharge of a Proton Exchange Membrane Electrolyzer: Investigation for Modeling Purposes. *Membranes* **2021**, *11*, 379, doi:10.3390/membranes11060379.